ACS APPLIED MATERIALS & INTERFACES

Research Article

Cite This: ACS Appl. Mater. Interfaces 2019, 11, 7242−7249

www.acsami.org

Multifunctional Self-Doped Nanocrystal Thin-Film Transistor Sensors

Dongsun Choi,[†] Mihyeon Park,[†] Juyeon Jeong,[†] Hang-Beum Shin,[‡] Yun Chang Choi,[†] and Kwang Seob Jeong*[,†]

[†]Department of Chemistry, Korea University, Seoul 02841, Republic of Korea

[‡]Corporate R&D, LG Chem., Ltd., 30, Magokjungang 10-ro, Gangseo-gu, Seoul 07796, Republic of Korea

Supporting Information

ABSTRACT: Self-doping in nanocrystals allows accessing higher quantum states. The electrons occupying the lowest energy state of the conduction band form a metastable state that is very sensitive to the electrostatic potential of the surface. Here, we demonstrate that the high charge sensitivity of the self-doped HgSe colloidal quantum dot solid can be used for sensing three different targets with different phases through self-doped HgSe nanocrystal/ZnO thin-film transistors: the environmental gases (CO_2 gas, NO gas, and H_2S gas); mid-IR photon; and biothiol (L-cysteine) molecules. The self-doped quantum dot solid detects the targets through different mechanisms. The physisorption of the CO_2 gas and the NO gas molecules, and the mid-IR photodetection show reversible processes, whereas the chemisorption of L-cysteine biothiol and H_2S gas molecules shows irreversible processes. Considering the quenching of mid-IR intraband photoluminescence of the HgSe colloidal quantum dot solid by the vibrational mode of the CO_2 gas molecule, sensing the CO_2 gas could be involved in the electronic-to-vibrational energy transfer. The target molecules are quantitatively analyzed, and the limits of detection for CO_2 and L-cysteine are 250 ppm and 10 nM, respectively, which are comparable to the performance of commercial detectors.

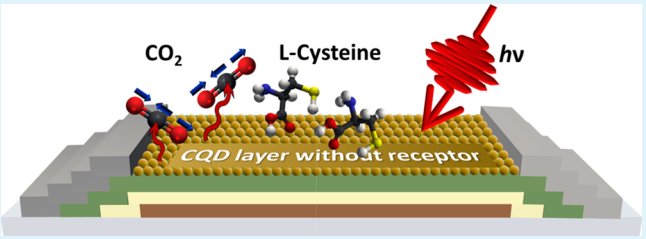

KEYWORDS: *self-doped nanocrystal, gas sensor, probe-free biosensor, mid-IR photodetector, TFT sensor*

INTRODUCTION

Chemical sensors have been intensively developed because of their versatile demands in healthcare, environmental pollution monitoring, and so on.[1−7] With respect to the sensor device fabrication, the solution-processed method has a merit in a highly cost-effective manufacturing process because there is no need for the process to be conducted at high temperature during the sensor fabrication unlike to other deposition methods.[6−13] Colloidal nanocrystals have been intensively studied for the sensor materials as well to monitor various targets, inferring that the change of the electronic property is readily changed by external perturbation.[2,6,7,14−19] For better sensitivity, various dimensions of nanocrystals such as the 0D,[20−23] 1D,[24−26] and 2D shaped,[27−29] have been examined along with different surface morphologies and electrical characteristics of the materials.[30−36] When it comes to generating charge carriers, the band-edge excitation is required in conventional colloidal quantum dots.[10,11,17,27−38] In this case, electrons remain in the valence band until photoexcitation triggers an electronic transition to elevate the electrons into the conduction band (CB) states. However, if the electrons already occupy the lowest electronic state of the CB, the electron only needs a few hundred meV energy for carrier generation.

Self-doped colloidal nanocrystals with doubly or singly charged (occupied) quantum states are recently reported by the Guyot-Sionnest group and our own group, which are explicitly different from the conventional quantum dots.[30,31,34,39−43] The self-doped colloidal nanocrystals are already filled with one or two electrons per state in the CB in the steady state.[39−43] Therefore, the electronic transition occurring in the discrete energy states of the CB is observed in the steady state without the bandgap transition. Because the electrons are at the CB, the electron wavefunctionsare not only confined to the nanocrystal, but also spatially distributed at the surface of the nanocrystal. Thus, both the singly occupied (charged) quantum state (SOQS) and the doubly occupied quantum state (DOQS) tend to be extremely sensitive to the surface charge. The high charge sensitivty of the self-doped nanocrytal is reflected in the change of optical strength of electronic transitions. Depending on the surface charge environment, the bandgap optical transition can be swiftly switched to the intraband transition and vice versa. The surface potential induced by the surface environment was previously reported to ±1.8 eV in case of HgS nanocrystals.[39] Thus, in

Received: September 18, 2018
Accepted: January 28, 2019
Published: January 28, 2019

DOI: 10.1021/acsami.8b16083
ACS Appl. Mater. Interfaces 2019, 11, 7242−7249

principle, the colloidal quantum dots (CQDs) with the SOQS and DOQS are highly possible to detect the charge variance arising from the interaction with external target molecules.[39−41] Therefore, we aimed to exploit the surface sensitivity of the self-doped nanocrystal for sensing the different targets. To note, the SOQS and DOQS are different from the trion state or biexciton states where the holes are present in the valence state.

Carbon dioxide (CO_2) gas, a major greenhouse gas, has been chosen as the first target molecule for the experiments because of its tremendous importance in the environment. To quantify the CO_2 gas in the atmosphere, it is known that nondispersive infrared (NDIR) sensors have been most widely used. The NDIR sensor is equipped with the spectroscopic components including an IR light source, a filter, and a detector. Because both the optical components and the detection parts are required in the system, reducing the sensor size or cost is essentially restricted. Therefore, for low-cost gas detection, a very novel design without the optical component is demanded.

For the biosensors, a fluorescent probe-free and mediator-free biosensing method is substantially important in detecting the target at a low manufacturing cost. Also, detection of L-cysteine ($HSCH_2$ $(NH_3)CHCO_2H$), which is one of the biothiol molecules and a semi-essential proteinogenic amino acid, is crucial because the lack of the L-cysteine in our body can induce fatal diseases such as neurotoxicity, liver damage, and leucocyte loss.[44] Fluorescent dye-based sensors typically require a continuous light source, monochromatic system for quantifying the fluorescence spectra at specific wavelength, and bulky optical components collecting the photons spread all around in space. If the fluorescent dye in the fluid is confined in the plastic tube or microchannel, the detecting intensity would be further deteriorated because of autofluoresce. For this reason, an electrochemical sensor platform, that is, the thin-film transistor (TFT) will be a good candidate of a molecule sensor with respect to miniaturization. The absence of the probe or mediator virtually simplifies the sensor fabrication and obviates potential issues regarding the small density of the active sites per unit area.

The high surface charge sensitivity of the self-doped colloidal quantum dots is an excellent physical property for the CO_2 gas and the biothiol molecule detection because it is known that the strength of the intraband transition, which is a peculiar optical property of the self-doped CQDs, can be reversibly tuned by manipulating the surface charge.[30,31,39−43] The on-and-off feature of the intraband transition by tuning the surface charge indicates that the electron occupation of the quantized electronic state is extremely sensitive to the surface charge that can be indeed exploited to monitor the charge variance induced by the interaction between the nanocrystal surface and the CO_2 gas or the L-cysteine molecules.

Here, we present the use of the self-doped HgSe nanocrystals for monitoring different targets: the CO_2 gas and the L-cysteine biothiol detection. To clearly understand the underlying mechanism, NO gas, H_2S gas, and mid-IR photon detection measurements were carried out as well.

To the best of our knowledge, this is the first self-doped CQD/ZnO TFT sensor for detecting multiphase target molecules by employing the high charge sensitivity of the doubly charged (or self-doped) colloidal nanocrystals.

EXPERIMENTAL METHOD

Materials. Mercury(II) chloride ($HgCl_2$, ACS, 99.5% min) was purchased from Alfa Aesar. Selenourea (98%), tetrachloroethylene (TCE, ACS reagent, ≥99.0%), ammonium sulfide solution (40−48 wt % in H_2O), and oleylamine (OLAm, technical grade, 70%) were purchased from Sigma-Aldrich.

HgSe CQD Synthesis. Selenourea solution is prepared by dissolving 12.6 mg of selenourea (0.1 mmol) in 1 mL of OLAm. The solution was degassed for 1 h under vacuum while maintaining 90 °C with 100 mTorr pressure. The selenourea solution turned into a clear solution. This selenium precursor solution turned to dark brown color when heated for 2 h at 180 °C under an argon atmosphere. A 27.2 mg of the mercury(II) chloride was utilized for mercury precursor solution using OLAm as the solvent. By degassing at 90 °C for 1 h and heating to 110 °C under argon, mercury(II) chloride was completely dissolved to OLAm and formed mercury precursor solution. The selenourea solution was injected into the mercury solution to grow mercury selenide nanocrystals. The mixture solution turned into dark immediately, and the size of nanocrystals was controlled by changing the reaction time. The nanocrystal growth was quenched by quickly adding 5 mL of OLAm in TCE solution. The product was precipitated by using methanol and centrifuged. The precipitate was redispersed in TCE when dried completely under ambient conditions. The ligand-exchanged HgSe nanocrystal was redispersed in D_2O for further characterization of the material.

Fourier Transform Infrared Absorption. The infrared absorption spectra of the samples were measured with 4 cm^{-1} resolution FTIR (Nicolet iS10, Thermo Scientific). The sample was dispersed in TCE to avoid other absorption spectra in the mid-infrared region.

X-ray Diffraction. A Rigaku D/Max Ultima III X-ray diffractometer with graphite-monochromatized Cu Kα (l = 1.4056 Å) was used to measure the lattice structure of HgSe. The measurement was operated under 40 kV and 30 mA irradiation power and 0.01° of sampling width.

^{1}H NMR. The synthesized HgSe nanocrystals were redissolved in the $CDCl_3$ solvent which contains 0.03 tetramethylsilane to measure ^{1}H NMR spectra with a Bruker 500 MHz spectrometer. The cysteine or hexamethylenediamine (HDA) ligand-exchanged HgSe CQDs were dispersed in D_2O or $CDCl_3$, respectively, before proton NMR measurement.

Device Fabrication. The bottom chromium gate was sputtered on the glass substrate, and the Al_2O_3 gate insulating layer and a ZnO active layer were in situ deposited with plasma-enhanced atomic layer deposition (PEALD). For the Al_2O_3 layer, the metal organic precursor, trimethyl aluminum flowed into the chamber through the bubbler with a carrier gas of argon, and the carbon dioxide (CO_2) as the oxidizing gas was used with a radio frequency plasma power density of 0.15 W/cm^2. The reaction was conducted on the substrate surface at the fixed temperature of 200 °C. The cycle was repeated 400 times to deposit a 45 nm thick Al_2O_3 layer. Likewise, ZnO was deposited 100 cycles with diethyl zinc and nitrous oxide (N_2O) to achieve a 10 nm thick ZnO layer. The novel weak reactant PEALD procedure to fabricate the stable ZnO TFT was reported previously.[45] Subsequently, aluminum was sputtered to form a 100 nm thick source and drain electrodes. The width (W) and length (L) of the TFT were W = 1500 μm and L = 200 μm, respectively. The initial I_d-V_g transfer characteristics were obtained by using HP 4156A semiconductor parametric analyzer. All the fabricated TFT devices were stored under a nitrogen atmosphere before use, and all the devices were prewashed with chloroform, ethanol, and acetone to remove any impurities on the active surface. The TFT devices were annealed at 150 °C on a hot plate for 1 h to remove the residual solvent and water before HgSe QD deposition. The OLAm-passivated HgSe CQDs in TCE (30 mg/mL) were deposited over the active layer using layer-by-layer spin-casting under N_2 at 3000 rpm for 15 s. The average QD film thickness was ∼200 nm. The solid-state ligand exchange was performed with 2 vol % HDA or 2 vol % ethanedithiol (EDT) solution in ethanol. The spin-casted HgSe film was washed with ethanol added dropwise to

DOI: 10.1021/acsami.8b16083
ACS Appl. Mater. Interfaces 2019, 11, 7242−7249

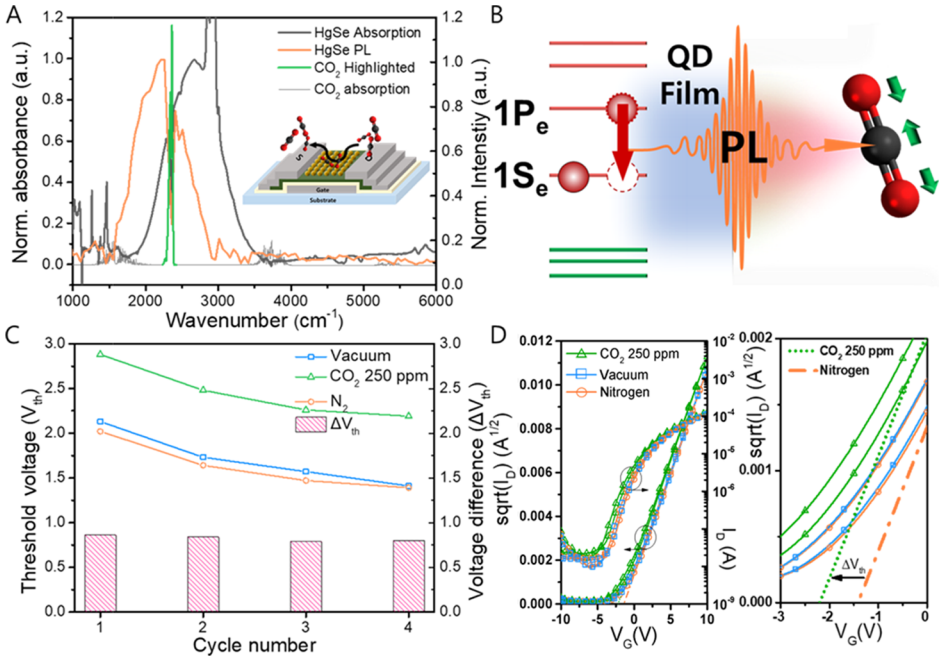

Figure 1. (A) Absorption and photoluminescence spectra of the HgSe CQD samples and the CO_2 gas IR absorption in the air background. The inset shows the schematic device geometry of the HgSe CQD/ZnO TFTgas sensor. (B) Schematic of intraband photoluminescence resonant with the CO_2 gas molecule (C) Reversible CO_2 gas detection under different atmospheres: vacuum; N_2; and CO_2 gas (250 ppm). (D) Transfer characteristics of the HgSe CQD/ZnO TFT gas sensor under different atmospheres and the zoomed-in at V_{th}.

remove the residual ligands at the same speed for 20 s. The entire film growth procedure was repeated five times to achieve optimize thickness. The HDA−HgSe CQD film and the EDT−HgSe CQD film were used for the biosensor and the gas sensor, respectively.

Gas Sensing. The gas sensor device was placed at the vacuum probe chamber for the CO_2 detection by using an HP 4156A semiconductor parameter analyzer. The drain current was measured by the gate voltage sweeping from −10 to 10 V in 0.1 V increment to characterize the I_d−V_g transfer curve. The device was monitored in cyclic order with vacuum (~10 mTorr), N_2 (~700 mTorr), and CO_2 (hundreds of ppm CO_2 mixture in N_2) environment. The vacuum chamber assures the exact gas response and produces a specific mixture ratio at the same pressure. The CO_2 gas detection measurement was performed in several cycles to ascertain the reversibility of the device. The probe chamber was purged with N_2 gas several times after CO_2 exposure to the device to remove CO_2 residuals in the detection chamber.

Mid-Wavelength Infrared Photodetectors. The sensor device was connected to an HP 4156A semiconductor analyzer for photosensing in the infrared region. An infrared emission source, Newport 6580, was focused on the active layer of the device by means of the off-axis mirror through the Ge optical filter, blocking the photons with the wavelength shorter than 2 μm. The irradiation area was 2.35 mm^2, and the temperature of the IR emitting source was 810 K.

Biomolecule Sensing. L-Cysteine in deionized water solution (2 mM to 500 μM) and L-cysteine in ethanol (1 μM to 10 nM) with different concentrations were prepared for biosensing. The device parameter was measured with an HP 4156A semiconductor parameter analyzer with the same voltage shift as the gas-sensing method. The prepared L-cysteine solution was dropped on the HgSe−HDA film and removed after 30 s. The residual water, or ethanol, was vacuum-dried for 15 min under 300 mTorr before each measurement.

Cyclic Voltammetry. The HgSe CQD film was formed over the interdigitated electrode by the drop-casting method. EDT was used as the cross-linker of the HgSe CQD film, and 0.1 M of tetrabutylammonium perchlorate in acetonitrile was used as the electrolyte. The platinum reference and counter electrodes were used, and 5 mV bias was applied to measure the conductive current with a scan rate of 0.03 V/s at −70 °C.

RESULTS AND DISCUSSION

Gas Sensors. The CO_2 gas measurement was performed by fabricating the HgSe CQD/ZnO TFT device in Figure 1A inset. The HgSe CQDs showing the absorption and photoluminescence (PL) at the mid-IR range were chosen as the sensor material to use the high sensitivity of the metastable DOQS. The DOQS swiftly changes the density of carrier inside the nanocrystal via nanocrystal surface potential change; it will be useful for sensing the minute change in charge induced by surrounding conditions.

To note, the CO_2 vibrational modes efficiently quench the mid-IR PL of HgSe CQDs at 2350 cm^{-1} as shown in Figure 1A. This is because the free CO_2 vibrational mode is resonant with the mid-IR intraband PL of the HgSe CQDs (Figure 1B). Considering the nonradiative decay rate of over 10^{-10} s of the HgTe CQDs arising from the electronic-to-vibrational energy transfer (EVET), the mid-IR intraband transition of the HgSe CQDs, in principle, is capable of efficiently detecting the vibrational modes of CO_2 gas molecules when they are around the nanocrystal sensor film.[39−43,46]

With these two properties of the high charge sensitivity and the efficient resonance in mid-IR, we have intensively focused on applying the metastable DOQS to the multifunctional sensors.

The fabrication details of the device are described in the Experimental Method section. Briefly, a colloidal HgSe CQD (Figures S1−S4) layer was spin-casted onto the staggered bottom gate TFT. A 10 nm thick ZnO layer (1500 × 200 μm) and a 45 nm thick Al_2O_3 layer are prepared by PEALD in situ and worked as the active and the dielectric layer, respectively. The bottom gate and top source and drain electrode are sputtered with Cr metal and Al metal, respectively. The as-

DOI: 10.1021/acsami.8b16083
ACS Appl. Mater. Interfaces 2019, 11, 7242−7249

synthesized OLAm ligand-capped HgSe CQDs were efficiently ligand exchanged with EDT ($HS(CH_2)_2SH$) for better carrier transport. In addition, the ligand exchange process facilitates the interaction between the nanocrystal film and the CO_2 gas molecules. The fabricated device is placed inside the vacuum probe station for the precise interrogation of a few hundreds of ppm of CO_2 molecules in Figure 2.

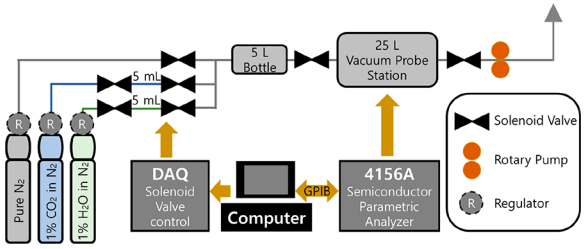

Figure 2. Schematic of the gas sensor measurement system used in the experiment. The CO_2 gas cylinder is replaced as other gases for specific gas detection; NO or H_2S, respectively.

The HgSe CQD/ZnO TFT sensor demonstrates that the transfer characteristic immediately responds to the adsorption of the gas molecule within a few voltage ranges. In the vacuum chamber, three atmospheric conditions were repeatedly provided: vacuum, nitrogen, and CO_2 mixed with nitrogen gas. The transfer characteristics were monitored (Figure 1D) under several gas conditions. Under a nitrogen atmosphere, the transfer characteristic does not change. However, in the presence of the CO_2 gas mixed with the nigrogen gas, the threshold voltage (V_{th}) is immediately shifted toward negative voltage. The CQD film becomes more positively charged by the surrounding CO_2 molecules, which causes the negative voltage shifts in transfer characteristic of the HgSe CQD/ZnO TFT device. Figure 1D (right, zoomed-in) represents the voltage shift by 0.8 V under 250 ppm CO_2 gas.

The sensor performance does not significantly change after being exposed to the ambient conditions, suggesting the strong air and humidity stability. Although water can affect the signal to some degree because of its hydrogen bonding at the surface of nanocrystals under ambient conditions, the signal variance resulting from the adsorption of the CO_2 gas still can be measured with high sensitivity. The capability of the sensor working under ambient conditions may result from the intrinsic air stability and humid stability of the HgSe nanocrystals that were previously reported.[38−40,43,47]

Iterative measurements confirmed the reproducibility of the results and revealed that the CO_2 gas detection with the sensor is reversible in Figure 1C. Although the V_{th} slightly shifts toward negative potential, the degree of V_{th} change remains constant with 0.83 (±0.05) V (Figure S5). The data shown in Figure 1D correspond to the fourth measurement in Figure

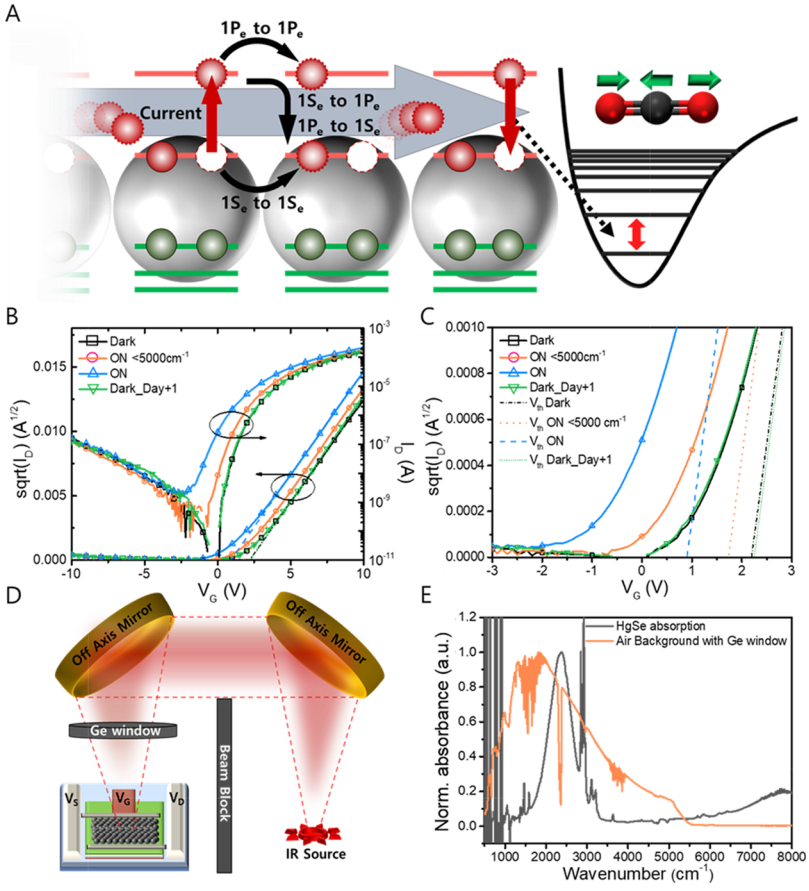

Figure 3. (A) Schematic diagram of possible electronic transition between $1P_e-1P_e$, $1S_e-1S_e$, $1S_e-1P_e$, and $1P_e-1S_e$ in the CQD films and the EVET mechanism between electronic transition of CQDs and the vibrational mode of the CO_2 gas molecule. (B) Transfer characteristic under mid-IR irradiation. (C) Zoomed-in at V_{th}. (D) A schematic diagram of the CQD/ZnO TFT for the mid-wavelength infrared photo detection system (E) Absorption spectra of HgSe CQDs (black) and air background with the Ge filter (orange).

DOI: 10.1021/acsami.8b16083
ACS Appl. Mater. Interfaces 2019, 11, 7242−7249

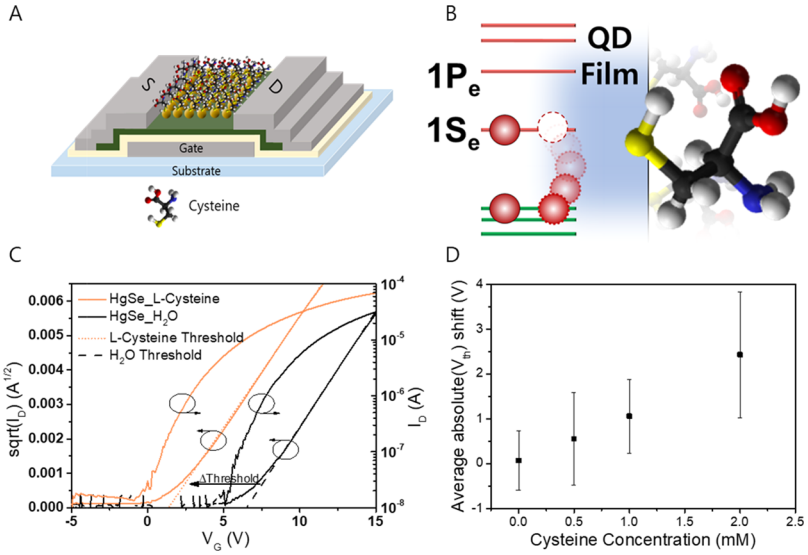

Figure 4. (A) Device geometry of the HgSe CQD/ZnO bio-TFT biosensor and the L-cysteine structure (B) Schematic diagram of the device surface after L-cysteine chemisorbed on the QD film (C) Transfer characteristics of the HgSe CQD/ZnO bio-TFT sensor with water solvent (black) and the L-cysteine (red). (D) Averaged V_{th} with different concentrations of the L-cysteine.

1C. The average V_{th} variance is ca. 0.83 V and the average range is from −1.6 V to −2.4 V.

The reversible sensing process observed in our system requires a different explanation because the conventional chemisorption CO_2 gas-sensing process shows the irreversible behavior (Figure S6) arising from the formation of carbamic acid ($RNHCO_2H$) because of the reaction between CO_2 gas and amine organic molecules.[47] Since the native OLAm ligands of HgSe CQDs are efficiently replaced by the short organic EDT during the HgSe CQD film fabrication, the possible residual functional group to interact with CO_2 is only thiol. If the thiol forms a covalent bond with the CO_2 gas, the reversible sensing would not be possible to occur. In addition, no clear hysteresis has been observed in the transfer characteristic, which explicitly contrasts the sulfur reduction/oxidation reaction which could be another chemisorption-based sensing process. Furthermore, the reversible signal with no hysteresis infers that defects of the TFT device are not the origin of the signal. Thus, based on the results, the physisorption of CO_2 gas onto the HgSe CQD film is indeed the mechanism in the HgSe CQD-sensitized CO_2 sensor.

The possible mechanism of the CO_2 sensing along with the physisorption is the EVET. The electronic transition of $1S_e-1P_e$ of the HgSe CQD is in the mid-IR regime where vibrational finger print modes are present. Because of the vibrational mode of the organic molecule, the radiative recombination is somewhat suppressed via the EVET. This idea is directly reflected in the result of the efficient quenching of the mid-IR PL, implying the resonance between the $1S_e-1P_e$ energy and the vibrational mode of the CO_2 molecule in our system.

In regards of the energy level of the $1S_e$ (−6.15 eV vs vacuum) and $1P_e$ (−5.65 eV vs vacuum) states of HgSe, it is highly possible that the HgSe CQDs serve as a conduction channel in some degree as well as the ZnO semiconductor film with a CB of −4.2 eV and a valence band of −7.5 eV. The electronic state position of HgSe CQDs with the intraband transition at 2500 cm^{-1} is experimentally identified by the electrochemical conduction current measurement in Figure S7. The possible electron conduction channels are the $1P_e-1P_e$, $1P_e-1S_e$, $1S_e-1P_e$, and $1S_e-1S_e$ between two different nanocrystals (Figure 3A). Therefore, if the electron and hole are created through the channel during the device running, the electron−hole pair created can interact with the vibrational modes of the CO_2 gas molecules, leading to the EVET (Figure 3A) process.

The mid-IR photodetection experiment confirms the active $1S_e-1P_e$ transition of the HgSe CQD solid, which is the main physical property of the CO_2 sensing. Under the incoherent mid-IR light source, the HgSe CQD/ZnO TFT sensor shows the shift of V_{th} by −0.6 V, demonstrating that the device properly runs under the mid-IR irradiation filtered with a Ge window (Figure 3B,C). The Ge filter allows only the infrared light of the wavelength longer than ∼1.8 μm (5500 cm^{-1}). To note, the intraband absorption spectrum of the HgSe CQDs (black) is well overlapped with the Ge-filtered infrared light source spectrum (red) in Figure 3D,E. The mid-IR irradiation gives rise to the formation of the intraband exciton in the HgSe CQDs, leading to the increase of the electric field strength applied to the ZnO layer. Interestingly, the recovery of the offset current from the infrared irradiation is significantly slow whereas the recovery of the offset current to the CO_2 gas is prompt.

To compare the CO_2-sensing mechanism with others, further gas sensing study has been carried out. The nitric oxide (NO) gas, a radical molecule and one of the major causes of the air pollution, was loaded into the gas measurement system.[48] The 1% of the NO gas diluted in N_2 gas fills the chamber and induces the shift of V_{th} by 5.5 V (Figure S8). To test the reversibility of the sensor, the vacuum was applied to the chamber. The transfer characteristic surprisingly recovers the original curve in some degree. To note, filling the system with N_2 gas does not make significant change in transfer characteristic. The second injection of the NO target gas with the identical concentration again results in the shift of V_{th} by 2.1 V. The third vacuum condition and N_2 gas condition recover the transfer characteristic to the original position. Based on the result, it is found that the HgSe CQD/ZnO TFT gas sensor indeed detects the NO gas.

DOI: 10.1021/acsami.8b16083
ACS Appl. Mater. Interfaces 2019, 11, 7242−7249

Lastly, the hydrogen sulfide (H_2S) gas was examined with the identical gas sensor system. The H_2S gas is colorless, flammable, and acutely toxic at high concentrations. It has been known that 100 ppm of H_2S gas can make people experience lacrimation, corneal opacity, and so forth.[49] The H_2S gas is also the byproduct of various industrial processes such as petroleum refining, requiring the detection of the H_2S gas with high precision. In general synthesis of colloidal nanocrystal, the H_2S gas is frequently used as a sulfur precursor for the nanocrystal shell growth. Thus, it is highly possible for the HgSe nanocrystals to react with the H_2S gas through chemisorption when they are exposed. In other words, the HgSe CQD/ZnO TFT gas sensor is indeed a suitable system for the H_2S gas sensing. Figure S9 represents the irreversible sensing for the H_2S gas. Under the exposure to the H_2S gas, the HgSe CQD/ZnO TFT sensor clearly shows the shift of V_{th} by ~1.4 V for the first measurement. The concentrations of the H_2S gas are 55 and 120 ppm in N_2 gas for the first and the second measurements, respectively. The second measurement induces further negative shift of the V_{th} by 0.5 V. Thus, based on the results above, it is demonstrated that the HgSe CQD/ZnO TFT sensor properly detects the CO_2, NO, and H_2S gases under room temperature via different mechanisms.

Biomolecule Sensors. The molecular sensing through the chemisorption as shown in the H_2S gas sensing can be expanded into the biomolecule sensing in the liquid phase. We tested the HgSe CQD/ZnO TFT sensor to detect L-cysteine. L-Cysteine was chosen in this experiment due to the structural merit as well as its importance in biological systems. L-Cysteine controls the glutathione levels in the body and plays an essential role in the functioning of the lung, brain, and liver detoxication.[44,50] It has a thiol and a carboxylic acid functional groups that can readily form the chemical bonding to the surface of HgSe nanocrystals. In this sensor device, HDA was used as a cross-linker instead of the EDT because the amine functional group of the HDA can be efficiently replaced by the thiol or carboxylate, which is intended to be the chemisorption mechanism for this L-cysteine detection (Figures 4A and S1). Figure 4B illustrates the surface effect of L-cysteine chemisorption on the QD film. To note, the cross-linker of the HgSe nanocrystals is only the difference between the L-cysteine biosensor and the gas sensor.

L-Cysteine solutions with different concentrations were prepared and the solution was dropped onto the surface of the active sensor layer followed by natural drying under ambient conditions. To remove the residual solvent, the device was placed into the antechamber at 300 mTorr vacuum for 15 min. Then, the transfer characteristics of the TFT sensor were carefully measured. Surprisingly, the V_{th} significantly shifts by 5.0 V at 2 mM of L-cysteine (Figure 4C).

The concentration of the L-cysteine was lowered from 2 mM to 500 μM for water solvent in Figure 4D. The limit of detection (LOD) is 500 μM under room temperature for the L-cysteine water solution (Figure S11). The transfer characteristic for the water treatment is also included in Figure 4C to clearly show the L-cysteine effect on the transfer characteristic. Interestingly, it was found that the LOD is substantially affected by the solvent. When the ethanol solvent is used, the LOD significantly improves to 10 nM (ΔV_{th} = 0.13 V) which is about 4 orders of magnitude smaller than that in water (Figure S12). Tentatively, we presume that this is attributed to the lack of residual solvent because of the high volatile ethanol. Further device optimization in the nanocrystal film morphology with various cross-linkers may improve the LOD of the device.

The mechanism for the biosensor intended is the chemisorption process. The L-cysteine with the two functional groups, thiol and carboxylic acid, can actively bind to the surface of the nanocrystals (Figures S10 and S13). In terms of its functional groups, the L-cysteine is similar to the mercaptopropionic acid that is a well-known cross-linker for enhancing the charge carrier transport process in the colloidal quantum dot solid. Hence, it is highly possible that the L-cysteine facilitates the charge transport by chemically binding to the surface of HgSe nanocrystals through the decrease of the interparticle distance. This hypothesis is supported by the irreversible shift in transfer characteristics of the TFT sensor in the presence of the L-cysteine molecules. All data we obtained consistently show a negative ΔV_{th}. The negative ΔV_{th} appears when more negative charges accumulate in the ZnO layer, resulting from the chemisorption of the L-cysteine.

The result in Figure 4D also informs that the direction of the V_{th} shift is consistent with that induced by the gas adsorption, indicating that the CO_2 gas, the H_2S gas adsorption, and the mid-IR photon irradiation facilitates the charge transport by forming the positive charge on the HgSe CQD layer, inducing negative charge accumulation at the ZnO layer.

CONCLUSIONS

In summary, we have demonstrated the CO_2 (g), NO (g), H_2S (g), L-cysteine (aq), and mid-IR photon sensing using solution-processable HgSe CQD/ZnO TFT sensors. In the self-doped HgSe CQDs filled with two electrons in the CB, the electron wave function is efficiently coupled to the surface of the nanocrystal, serving as an efficient charge probe monitoring the dielectric variation resulting from the target molecule adsorption. The ZnO TFT platform has detected the potential change of the HgSe CQDs which is effectively converted into electrical signals without significant energy conversion losses. The CO_2 adsorption to the HgSe CQD film leads to the negative threshold voltage shift in the transfer characteristic by 0.82 V under 250 ppm CO_2 at room temperature. Strikingly, the shift is reversible with high reproducibility, inferring that the CO_2 gas is physisorbed onto the nanocrystal film and possibly attributed to the intraband electronic transition-to-vibrational mode of the CO_2 gas energy transfer. The negative shift of V_{th} is consistent with the result arising from the mid-IR photon detection with the identical device, representing that the CO_2 adsorption facilitates the carrier transport in the HgSe CQD/ZnO TFT device. To exploit the charge sensitivity of the HgSe nanocrystals with the DOQS, we demonstrated the capability of the TFT sensor to monitor the concentration of L-cysteine solution at room temperature. The LODs of the sensor are 10 nM and 500 μM for the L-cysteine in ethanol solution and in water solution, respectively. Surprisingly, the LOD of the CO_2 gas sensor is comparable to that of the commercial NDIR CO_2 sensor whereas the current LOD of the biosensor has a room for improvement in device optimization. The self-doped colloidal nanocrystal will serve as promising sensor materials with respect to its versatile usages in multifunctional gas, photon, and biomolecule detections.

DOI: 10.1021/acsami.8b16083
ACS Appl. Mater. Interfaces 2019, 11, 7242−7249

■ ASSOCIATED CONTENT

Supporting Information

The Supporting Information is available free of charge on the ACS Publications website at DOI: 10.1021/acsami.8b16083.

IR, TEM,X-ray diffraction, and UV/Vis absorption data of HgSe CQDs, reversible sensor transfer characteristic curves, CO_2 gas exposer to the HgSe CQD/ZnO device, 1 mM to 10 nM L-cysteine concentration transfer characteristics, low L-cysteine concentration V_{th} shift, conduction current measurement of HgSe CQD sample, and the ^{1}H NMR spectrum of HgSe CQDs- L-cysteine- (PDF)

■ AUTHOR INFORMATION

Corresponding Author

*E-mail: kwangsjeong@korea.ac.kr.

ORCID

Kwang Seob Jeong: 0000-0003-3246-7599

Funding

This research was supported by the Basic Science Research Program through the National Research Foundation of Korea (NRF) funded by the Ministry of Science, ICT, & Future Planning (NRF-2016R1C1B2013416) and LG Chem. Ltd. The author gratefully acknowledge the use of the facilities of the Korea Basic Science Institute (KBSI).

Notes

The authors declare no competing financial interest.

■ REFERENCES

(1) Rodrigo, D.; Limaj, O.; Janner, D.; Etezadi, D.; Garcia de Abajo, F. J.; Pruneri, V.; Altug, H. Mid-Infrared Plasmonic Biosensing with Graphene. *Science* **2015**, *349*, 165−168.

(2) Bai, J.; Zhou, B. Titanium Dioxide Nanomaterials for Sensor Applications. *Chem. Rev.* **2014**, *114*, 10131−10176.

(3) Someya, T.; Dodabalapur, A.; Huang, J.; See, K. C.; Katz, H. E.; Katz, H. E. Chemical and Physical Sensing by Organic Field-Effect Transistors and Related Devices. *Adv. Mater.* **2010**, *22*, 3799−3811.

(4) Janata, J.; Josowicz, M. Conducting Polymers in Electronic Chemical Sensors. *Nat. Mater.* **2003**, *2*, 19−24.

(5) McDonagh, C.; Burke, C. S.; MacCraith, B. D. Optical Chemical Sensors. *Chem. Rev.* **2008**, *108*, 400−422.

(6) Liu, H.; Li, M.; Voznyy, O.; Hu, L.; Fu, Q.; Zhou, D.; Xia, Z.; Sargent, E. H.; Tang, J. Physically Flexible, Rapid-Response Gas Sensor Based on Colloidal Quantum Dot Solids. *Adv. Mater.* **2014**, *26*, 2718−2724.

(7) Saran, R.; Curry, R. J. Lead Sulphide Nanocrystal Photodetector Technologies. *Nat. Photonics* **2016**, *10*, 81−92.

(8) Hetsch, F.; Zhao, N.; Kershaw, S. V.; Rogach, A. L. Quantum Dot Field Effect Transistors. *Mater. Today* **2013**, *16*, 312−325.

(9) Murray, C. B.; Kagan, B.; Bawendi, M. G. Synthesis and Characterization of Monodisperse Nanocrystals and Close-Packed Nanocrystal Assembles. *Annu. Rev. Mater. Sci.* **2000**, *30*, 545−610.

(10) Oertel, D. C.; Bawendi, M. G.; Arango, A. C.; Bulović, V. Photodetectors Based on Treated CdSe Quantum-Dot Films. *Appl. Phys. Lett.* **2005**, *87*, 213505.

(11) Talapin, D. V.; Murray, C. B. PbSe Nanocrystal Solids for n- and p-Channel Thin Film Field-Effect Transistors. *Science* **2005**, *310*, 86−89.

(12) Kolmakov, A.; Zhang, Y.; Cheng, G.; Moskovits, M. Detection of CO and O_2 Using Tin Oxide Nanowire Sensors. *Adv. Mater.* **2003**, *15*, 997−1000.

(13) Liu, H.; Zhang, W.; Yu, H.; Gao, L.; Song, Z.; Xu, S.; Li, M.; Wang, Y.; Song, H.; Tang, J. Solution-Processed Gas Sensors Employing SnO_2 Quantum Dot/MWCNT Nanocomposites. *ACS Appl. Mater. Interfaces* **2016**, *8*, 840−846.

(14) Walker, G. W.; Sundar, V. C.; Rudzinski, C. M.; Wun, A. W.; Bawendi, M. G.; Nocera, D. G. Quantum-Dot Optical Temperature Probes. *Appl. Phys. Lett.* **2003**, *83*, 3555−3557.

(15) Medintz, I. L.; Uyeda, H. T.; Goldman, E. R.; Mattoussi, H. Quantum Dot Bioconjugates for Imaging, Labelling and Sensing. *Nat. Mater.* **2005**, *4*, 435−446.

(16) Yue, Z.; Lisdat, F.; Parak, W. J.; Hickey, S. G.; Tu, L.; Sabir, N.; Dorfs, D.; Bigall, N. C. Quantum-Dot-Based Photoelectrochemical Sensors for Chemical and Biological Detection. *ACS Appl. Mater. Interfaces* **2013**, *5*, 2800−2814.

(17) Sun, H.; Wu, L.; Wei, W.; Qu, X. Recent Advances in Graphene Quantum Dots for Sensing. *Mater. Today* **2013**, *16*, 433−442.

(18) Talapin, D. V.; Lee, J.-S.; Kovalenko, M. V.; Shevchenko, E. V. Prospects of Colloidal Nanocrystals for Electronic and Optoelectronic Applications. *Chem. Rev.* **2010**, *110*, 389−458.

(19) Yang, S.; Zhao, N.; Zhang, L.; Zhong, H.; Liu, R.; Zou, B. Field-Effect Transistor-Based Solution-Processed Colloidal Quantum Dot Photodetector with Broad Bandwidth into Near-Infrared Region. *Nanotechnology* **2012**, *23*, 255203.

(20) Zhang, C.-Y.; Yeh, H.-C.; Kuroki, M. T.; Wang, T.-H. Single-quantum-dot-based DNA nanosensor. *Nat. Mater.* **2005**, *4*, 826−831.

(21) Epifani, M.; Comini, E.; Díaz, R.; Andreu, T.; Genç, A.; Arbiol, J.; Siciliano, P.; Faglia, G.; Morante, J. R. Solvothermal, Chloroalkoxide-Based Synthesis of Monoclinic WO_3 Quantum Dots and Gas-Sensing Enhancement by Surface Oxygen Vacancies. *ACS Appl. Mater. Interfaces* **2014**, *6*, 16808−16816.

(22) Nazzal, A. Y.; Qu, L.; Peng, X.; Xiao, M. Photoactivated CdSe Nanocrystals as Nanosensors for Gases. *Nano Lett.* **2003**, *3*, 819−822.

(23) Chen, M.; Lu, H.; Abdelazim, N. M.; Zhu, Y.; Wang, Z.; Ren, W.; Kershaw, S. V.; Rogach, A. L.; Zhao, N. Mercury Telluride Quantum Dot Based Phototransistor Enabling High-Sensitivity Room-Temperature Photodetection at 2000 nm. *ACS Nano* **2017**, *11*, 5614−5622.

(24) Kolmakov, A.; Moskovits, M. Chemical Sensing and Catalysis by One-Dimensional Metal-Oxide Nanostructures. *Annu. Rev. Mater. Res.* **2004**, *34*, 151−180.

(25) Kong, J.; Franklin, N. R.; Zhou, C.; Chapline, M. G.; Peng, S.; Cho, K.; Dai, H. Nanotube Molecular Wires as Chemical Sensors. *Science* **2000**, *287*, 622−625.

(26) Comini, E.; Faglia, G.; Sberveglieri, G.; Pan, Z.; Wang, Z. L. Stable and Highly Sensitive Gas Sensors Based on Semiconducting Oxide Nanobelts. *Appl. Phys. Lett.* **2002**, *81*, 1869−1871.

(27) Yuan, W.; Liu, A.; Huang, L.; Li, C.; Shi, G. High-Performance NO_2 Sensors Based on Chemically Modified Graphene. *Adv. Mater.* **2013**, *25*, 766−771.

(28) Ou, J. Z.; Ge, W.; Carey, B.; Daeneke, T.; Rotbart, A.; Shan, W.; Wang, Y.; Fu, Z.; Chrimes, A. F.; Wlodarski, W.; Russo, S. P.; Li, Y. X.; Kalantar-zadeh, K. Physisorption-Based Charge Transfer in Two-Dimensional SnS_2 for Selective and Reversible NO_2 Gas Sensing. *ACS Nano* **2015**, *9*, 10313−10323.

(29) Comini, E.; Guidi, V.; Malagù, C.; Martinelli, G.; Pan, Z.; Sberveglieri, G.; Wang, Z. L. Electrical Properties of Tin Dioxide Two-Dimensional Nanostructures. *J. Phys. Chem. B* **2004**, *108*, 1882−1887.

(30) Guyot-Sionnest, P. Mid-Infrared Photoluminescence of CdS and CdSe Colloidal Quantum Dots. *ACS Nano* **2016**, *10*, 2225−2231.

(31) Deng, Z.; Jeong, K. S.; Guyot-Sionnest, P. Colloidal Quantum Dots Intraband Photodetectors. *ACS Nano* **2014**, *8*, 11707−11714.

(32) Robin, A.; Livache, C.; Ithurria, S.; Lacaze, E.; Dubertret, B.; Lhuillier, E. Surface Control of Doping in Self-Doped Nanocrystals. *ACS Appl. Mater. Interfaces* **2016**, *8*, 27122−27128.

(33) Brown, P. R.; Kim, D.; Lunt, R. R.; Zhao, N.; Bawendi, M. G.; Grossman, J. C.; Bulović, V. Energy Level Modification in Lead Sulfide Quantum Dot Thin Films through Ligand Exchange. *ACS Nano* **2014**, *8*, 5863−5872.

(34) Shen, G.; Guyot-Sionnest, P. HgS and HgS/CdS Colloidal Quantum Dots with Infrared Intraband Transitions and Emergence of a Surface Plasmon. *J. Phys. Chem. C* **2016**, *120*, 11744−11753.
(35) Zhang, Y.-Y.; Zhou, H.; Wu, P.; Zhang, H.-R.; Xu, J.-J.; Chen, H.-Y. In Situ Activation of CdS Electrochemiluminescence Film and Its Application in H_2S Detection. *Anal. Chem.* **2014**, *86*, 8657−8664.
(36) Tang, X.; Wu, G. f.; Lai, K. W. C. Plasmon Resonance Enhanced Colloidal HgSe Quantum Dot Filterless Narrowband Photodetectors for Mid-Wave Infrared. *J. Mater. Chem. C* **2017**, *5*, 362−369.
(37) Li, M.; Zhou, D.; Zhao, J.; Zheng, Z.; He, J.; Hu, L.; Xia, Z.; Tang, J.; Liu, H. Resistive Gas Sensors Based on Colloidal Quantum Dot (CQD) Solids for Hydrogen Sulfide Detection. *Sens. Actuators, B* **2015**, *217*, 198−201.
(38) Ning, Z.; Voznyy, O.; Pan, J.; Hoogland, S.; Adinolfi, V.; Xu, J.; Li, M.; Kirmani, A. R.; Sun, J.-P.; Minor, J.; Kemp, K. W.; Dong, H.; Rollny, L.; Labelle, A.; Carey, G.; Sutherland, B.; Hill, I.; Amassian, A.; Liu, H.; Tang, J.; Bakr, O. M.; Sargent, E. H. Air-Stable n-Type Colloidal Quantum Dot Solids. *Nat. Mater.* **2014**, *13*, 822−828.
(39) Yoon, B.; Jeong, J.; Jeong, K. S. Higher Quantum State Transitions in Colloidal Quantum Dot with Heavy Electron Doping. *J. Phys. Chem. C* **2016**, *120*, 22062−22068.
(40) Jeong, J.; Yoon, B.; Kwon, Y.-W.; Choi, D.; Jeong, K. S. Singly and Doubly Occupied Higher Quantum States in Nanocrystals. *Nano Lett.* **2017**, *17*, 1187−1193.
(41) Choi, D.; Yoon, B.; Kim, D.-K.; Baik, H.; Choi, J.-H.; Jeong, K. S. Major Electronic Transition Shift from Bandgap to Localized Surface Plasmon Resonance in $Cd_xHg_{1-x}Se$ Alloy Nanocrystals. *Chem. Mater.* **2017**, *29*, 8548−8554.
(42) Park, M.; Choi, D.; Choi, Y.; Shin, H.-b.; Jeong, K. S. Mid-Infrared Intraband Transition of Metal Excess Colloidal Ag_2Se Nanocrystals. *ACS Photonics* **2018**, *5*, 1907−1911.
(43) Jeong, K. S.; Deng, Z.; Keuleyan, S.; Liu, H.; Guyot-Sionnest, P. Air-Stable n-Doped Colloidal HgS Quantum Dots. *J. Phys. Chem. Lett.* **2014**, *5*, 1139−1143.
(44) Janáky, R.; Varga, V.; Hermann, A.; Saransaari, P.; Oja, S. S. Mechanisms of L-Cysteine Neurotoxicity. *Neurochem. Res.* **2000**, *25*, 1397−1405.
(45) Mourey, D. A.; Zhao, D. A.; Sun, J.; Jackson, T. N. Fast PEALD ZnO Thin-Film Transistor Circuits. *IEEE Trans. Electron Devices* **2010**, *57*, 530−534.
(46) Keuleyan, S.; Kohler, J.; Guyot-Sionnest, P. Photoluminescence of Mid-Infrared HgTe Colloidal Quantum Dots. *J. Phys. Chem. C* **2014**, *118*, 2749−2753.
(47) Hahn, M. W.; Jelic, J.; Berger, E.; Reuter, K.; Jentys, A.; Lercher, J. A. Role of Amine Functionality for CO_2 Chemisorption on Silica. *J. Phys. Chem. B* **2016**, *120*, 1988−1995.
(48) Kreuzer, L. B.; Patel, C. K. N. Nitric Oxide Air Pollution: Detection by Optoacoustic Spectroscopy. *Science* **1971**, *173*, 45−47.
(49) Reiffenstein, R. J.; Hulbert, W. C.; Roth, S. H. Toxicology of Hydrogen Sulfide. *Annu. Rev. Pharmacol. Toxicol.* **1992**, *32*, 109−134.
(50) Forshammar, J.; Block, L.; Lundborg, C.; Biber, B.; Hansson, E. Naloxone and Ouabain in Ultralow Concentrations Restore Na+/K +-ATPase and Cytoskeleton in Lipopolysaccharide-treated Astrocytes. *J. Biol. Chem.* **2011**, *286*, 31586−31597.

DOI: 10.1021/acsami.8b16083
ACS Appl. Mater. Interfaces 2019, 11, 7242−7249